

On the Physics of Hadronic Blazar Emission Models

A. Reimer

Leopold-Franzens-Universität Innsbruck, Institut für Theoretische Physik, und Institut für Astro- und Teilchenphysik, 6020 Innsbruck, Austria

E-mail: anita.reimer@uibk.ac.at

Abstract. The material of relativistic jets of active galactic nuclei is composed of leptons and hadrons. If a significant fraction of the overall jet power is converted into energizing protons to relativistic energies, along with the leptons, hadronic interactions play a role in converting particle energy into radiation and neutrino production. I will discuss the physics and some properties of hadronic blazar emission models in the framework of recent developments in this field.

1. Introduction

Active Galactic Nuclei (AGN) are among the most luminous objects in the universe. Only a small percentage ($\sim 10\%$) of them turn out to possess prominent jets which continuously transport material from the innermost region of the AGN to kpc-, sometimes even Mpc-scale distances with relativistic speed. Following the unification scheme of such radio-loud AGN, flat spectrum radio-quasars (FSRQs) and BL Lac objects (commonly referred to as “blazars”) are those which are observed under a small viewing angle with respect to the jet axis, whereas those observed at large viewing angles are classified as Fanaroff Riley I and II radio galaxies, hence commonly considered as the blazars’ parent populations (e.g., [41]). Such jets of AGN are observed as broadband photon sources, being detected from the radio band up to very-high energy (VHE) gamma-ray energies. The census of GeV-detected blazars has dramatically increased from less than 100 blazars as detected by the EGRET instrument onboard the *Compton Gamma-Ray Observatory* to nearly 10^3 LAT (=Large Area Telescope)-detected high-latitude objects that have been associated with AGN since the launch of the *Fermi* satellite about two years ago [4]. The (nearly permanent) survey observation mode of the LAT-instrument onboard *Fermi* has triggered many follow-up observations of selected AGN also with the permanently improving instrument capabilities of modern Cherenkov-telescopes (ACTs). As a result, blazars of all subtypes (FSRQs, all types of BL Lac objects: low-frequency peaked BL Lacs (LBLs), intermediate-frequency peaked BL Lacs (IBLs), high-frequency-peaked BL Lacs (HBLs)) have meanwhile been detected at VHEs, thereby nearly doubling the census of blazars detected in this extreme photon energy band during the last two years. Most of the photon spectral energy distribution (SED) of blazars is dominated by radiation from non-thermal particle distributions in the jet. This is because the jet radiation is strongly beamed in these objects, thereby overwhelming any possible thermal signatures from the accretion disk, dusty torus or host galaxy.

Among the most striking properties of blazars is their variability at all wavelengths with variability time scales from weeks to months in the radio domain, down to even minutes in a few

cases at VHEs (e.g., PKS 2155-304 [7], Mkn 501 [9]). Such extreme behaviour occurs in general during an enhanced flux and variability stage. The greatly improved sensitivity of gamma-ray instruments, however, allows meanwhile to detect a number of blazars at various variability stages including a quiescent non-variable state (see e.g., [2] for a study of gamma-ray variability properties of blazars).

The SED of jetted AGN consists of two broad components. The low-energy component is in general attributed to synchrotron radiation from relativistic electrons (e^-) and positrons (e^+) in a relativistically moving “blob” in the jet. The origin of the high-energy hump is still a matter of debate, depending strongly on the overall jet composition (see below). Recently, a new classification scheme for a spectral classification of blazars has been proposed based on the synchrotron peak of their broadband SED [3], and independent of being a BL Lac object or a quasar. Here, low-synchrotron-peaked blazars (LSPs) have their low-energy peak at $\nu_{s,peak} < 10^{14}\text{Hz}$, intermediate-synchrotron-peaked blazars (ISPs) at $10^{14} \leq \nu_{s,peak} \leq 10^{15}\text{Hz}$, and high-synchrotron-peaked (HSPs) at $\nu_{s,peak} > 10^{15}\text{Hz}$.

Despite the rapid increase of photon data in recent years many questions on the jet physics of AGN are still unsolved, among them the composition of their relativistic particle populations and their properties.

Depending on this jet matter composition two types of emission models have emerged during the last decade. So-called “leptonic” models consider relativistic e^-e^+ as the emitting relativistic particle population, while in so-called “hadronic” emission models the relativistic jet material is composed of relativistic protons (p) and e^- . In both types of jet material cold pairs and/or protons may exist as well, allowing charge neutrality to be fulfilled. So-called “lepto-hadronic emission models” follow the same physics as “hadronic emission models”. In the following I will therefore follow the historical path and use the term “hadronic model” for describing radiation from relativistic e^-p jet matter compositions.

The historical motivation to consider relativistic protons in AGN jets is linked with the observation of ultra-high energy cosmic rays (UHECRs) up to several tens of EeV impinging the Earth from all directions. Indeed, AGN jets are among the prime candidate sources for these extremely energetic events. They fulfill all required criteria (e.g., [17]): Luminous AGN jets are located within the GZK horizon (~ 50 Mpc), provide sufficient power to potentially accelerate the charged jet particles beyond EeV scales and contribute significantly to the overall observed cosmic ray energetics, and fulfill the so-called “Hillas criterium” [21]. Yet, deflections of the charged particles in the intergalactic magnetic field complicate a direct signature of the sources in the observed CR distributions.

Observational indications of the existence of protons in AGN jets are meanwhile accumulating from various directions: If the observed X-ray cavities emerging from radio AGN jets in galaxy clusters (e.g., Cyg A; [42, 20]) are in pressure equilibrium with the intercluster medium, a significant matter component in those bubbles beyond of what pairs can provide is required. The non-detection of the predicted soft X-ray excess radiation and X-ray precursors to blazar flares from bulk Comptonization of cold pairs in quasars with strong accretion disk radiation puts serious limits to the jet’s overall pair content (e.g., [39]). The modeling of blazar SEDs with leptonic models reveals a total luminosity in pairs and magnetic field that is significantly less than the observed radiative power L_{rad} in the comoving frame, L_{rad}/Γ^2 (e.g., [16]), with Γ the bulk Lorentz factor. Energy conservation thus requires the existence of nucleons and/or nuclei in such blazar jets, a robust lower limit of the total jet power is given by $L_{jet} > L_{rad}/\Gamma^2$. The role of pairs as jet energy carrier is therefore negligible, making hadrons the energetically and dynamically dominating matter component in blazar jets. What remains unclear so far are the properties of this hadron component: Is this hadron population (partly) relativistic, or entirely cold? If the former, what is the fractional relativistic hadron to electron ratio, and what are the maximum energies reached? Where are those relativistic nucleons

produced/accelerated and by which mechanism(s)? Where are the observational signatures of these relativistic hadrons in AGN jet spectra? The application of hadronic emission models to blazar SEDs is thus required to answer those questions at least partly.

2. Photon and particle production in hadronic blazar emission models

In hadronic jet emission models, both a relativistic electron and proton population exist in the emitting magnetized¹ "blob" which itself moves with relativistic speed βc along the jet axis. As a consequence, leptonic and hadronic² processes must be fully considered: synchrotron radiation and inverse Compton scattering of charged particles, photon-photon and Bethe-Heitler pair production, photomeson production, inelastic nucleon-nucleon interactions, neutron decay. In this sense, leptonic emission models constitute a part of hadronic emission models.

Hadronic models where nucleon-nucleon interactions play an integral part have been proposed occasionally over the last decades (e.g., [12, 31, 11]). In those scenarios (star-jet interaction, relativistic blast wave, jet-red giant interaction, etc.) extremely dense target media for proton-proton interactions are considered. In the following I shall, however, focus on the more common hadronic emission models where particle-photon interactions dominate over particle-particle interactions (e.g., [23, 32, 13, 27, 29, 30, 10]).

Figure 1 shows the relevant energy loss rates of protons which is compared to the energy loss rates for electrons in Figure 2. Overall, the photon production rate from electron interactions is in general larger than from proton interactions, electrons lose their energy more rapidly in dense radiative environments than protons. This makes electrons efficient radiators, nucleons - irrespective of whether they are cold or relativistic - are excellent energy carriers. Both properties are required in AGN jets.

Because the interaction threshold for Bethe-Heitler pair production is located at lower energies (with center-of-momentum frame (CMF) energy $\sqrt{s} = (m_p + 2m_e)c^2$) than for photomeson production (with CMF energy $\sqrt{s} = (m_p + m_\pi)c^2$), energy loss rates below the pion photoproduction threshold are dominated by pair production. Above this latter threshold energy losses from photomeson production typically dominate over those from pair production due to their several orders of magnitude greater inelasticity, ranging between ~ 0.2 in steep power-law target photon fields to nearly ~ 0.5 in very flat target photon fields (see Figure 3; [37]). In contrast to pair production on protons, photomeson production allows proton to neutron conversion (and vice versa) via charge exchange (e.g. [28])³. As a consequence collimated neutron beams may form [19, 10] which can be used to transport a significant portion of the initial energy to large distances from the black hole.

There are various target photon fields for particle-photon interactions in AGN jets: the internal jet synchrotron photon field [23, 29, 30], and fields external to the jet such as direct accretion disk radiation [32, 13], jet or accretion disk radiation reprocessed in the BLR [10], or radiation by the dusty torus. The secondary (stable) particles from those are γ -rays, pairs and neutrinos (ν). For power-law target photon fields the resulting γ -ray to ν energy content E_γ/E_ν^4 lies around unity ($\sim 1 - 1.4$) for a wide spectral index range, with 10% (8%) for

¹ In the following I consider the magnetic field uniformly and isotropically distributed in the comoving "blob" frame for simplicity. Other scenarios may consider stochastic magnetic fields (e.g., [24] in the case of GRBs) giving rise to jitter radiation in the relativistic regime.

² The following restricts to proton interactions only. Heavy nuclei are generally more likely to photo-disintegrate into protons and neutrons in dense radiation fields rather than suffer photomeson production losses. Photo-disintegration has, however, recently been shown to fail providing an efficient process for VHE photon production [8], leaving protons as a more efficient photon producer.

³ e.g., in hadronic $p\gamma$ -interactions 30%-70% of the initial protons are converted into neutrons [28]

⁴ e^\pm are assumed to be 100% radiatively efficient.

steep power-laws to 25% (20%) in case of flat power-laws of the initial proton energy stored into photons (neutrinos) (see Figure 4; [37]). The average photon and neutrino energy per injected nucleon energy is dependent on the CMF energy where the dominant part of photomeson production takes place. In steep target photon spectra this is rather around the Δ -resonance region while for hard target photon fields the multipion production region plays a significant role [25]. Consequently the average photon (neutrino) energy ranges from 6% (4%) the injected nucleon energy in steep target photon fields to a fraction of % in flat target photon spectra (see Figure 5; [37]).

Figure 1 compares also the energy loss time scales from synchrotron radiation of muons in typically proposed blazar magnetic field strengths⁵ with their decay time scales. Obviously, for sufficient energetic muons, such as e.g., produced in photomeson production initiated by UHE protons, muon synchrotron losses prior to their decay can not be neglected (e.g., [34]). This applies similarly also to charged pions and kaons (e.g., [30]). Indeed, if field strengths are sufficiently high (\geq several tens of Gauss) p-[27, 5] μ^\pm - and π^\pm -synchrotron radiation may constitute an important high energy photon component.

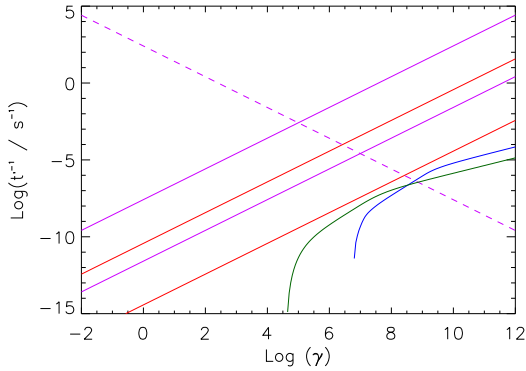


Figure 1. Energy loss rates (in the jet frame) for protons due to synchrotron radiation (red) in a 1 G (lower) and 100 G (upper curve) magnetic field, photomeson production (blue) and Bethe-Heitler pair production (green) in a broken power-law target photon field with photon index 1.5 below the break energy of 0.1 eV (jet frame) and 2.25 above this energy and with a total energy density $u_\gamma = 10^{11} \text{eV/cm}^3$. The magenta solid line represents synchrotron losses of charged muons in a 1 G (lower) and 100 G (upper curve) magnetic field in comparison to their decay time scale (magenta dashed line).

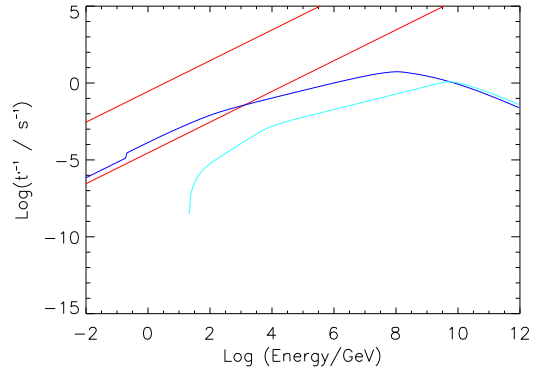


Figure 2. Energy loss rates (in the jet frame) for electrons due to synchrotron radiation (red) in a 1 G (lower) and 100 G (upper) magnetic field and inverse Compton scattering (dark blue) in comparison to photon-photon pair production (light blue) in a broken power-law target photon field with photon index 1.5 below the break energy of 0.1 eV (jet frame) and 2.25 above this energy and with a total energy density $u_\gamma = 10^{11} \text{eV/cm}^3$.

Very high energy photons (produced, e.g., through decay of photomeson produced π s) may find the emission region optically thick (see Figure 2): a pair cascade then develops which

⁵ except for one-zone SSC models where broadband SED modeling in general requires significantly lower field strengths

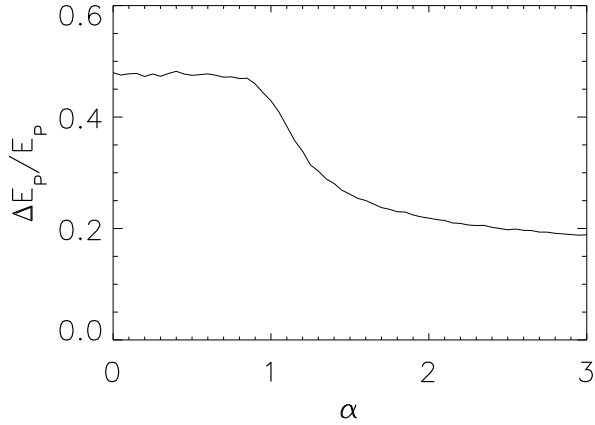


Figure 3. Inelasticity for photomeson production in power-law target photon fields with photon index α [37].

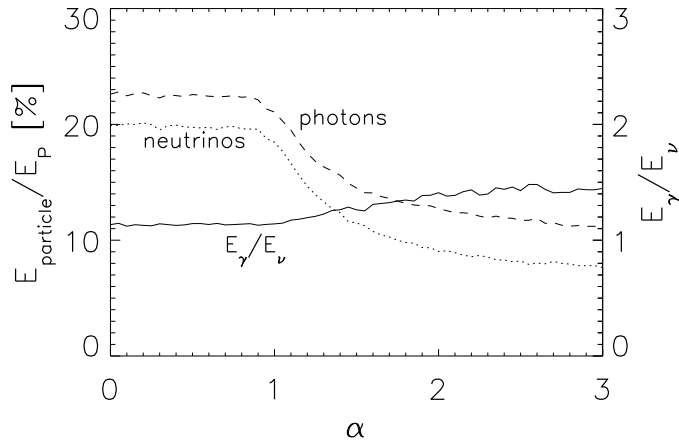


Figure 4. Photon and neutrino energy content per primary nucleon energy in photomeson production in power-law target photon fields with photon index α [37]. e^\pm are assumed to be 100% radiatively efficient.

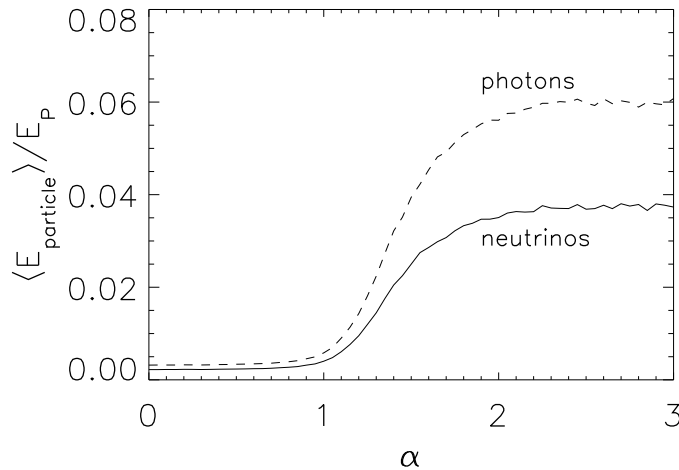


Figure 5. Average photon and neutrino energy per injected nucleon energy in photomeson production in power-law target photon fields with photon index α [37]. e^\pm are assumed to be 100% radiatively efficient.

redistributes the power from very high to lower energies. Depending on the overall field to photon energy density in the emission region synchrotron- [23, 29, 30, 10] or inverse Compton supported pair cascades [10] may dominate (see Figure 2). Electromagnetic cascades can be initiated by photons from π^0 -decay (“ π^0 -cascade”), electrons from the $\pi^\pm \rightarrow \mu^\pm \rightarrow e^\pm$ decay (“ π^\pm -cascade”),

p -synchrotron photons (“ p -synchrotron cascade”), and μ^- , π^- and K -synchrotron photons (“ μ^\pm -synchrotron cascade”). Ref. [29] and ref. [30] have shown that the “ π^0 cascades” and “ π^\pm cascades” generate rather featureless γ -ray spectra, in comparison to “ p -synchrotron cascades” and “ μ^\pm -synchrotron cascades” which produce distinct features in the high energy SED.

Generally, hadronic AGN emission models also consider all leptonic processes (including inverse Compton scattering off low energy photons) owing to the presence of ultrarelativistic e^- in the emission region. For sufficient high field strengths, any inverse Compton component is, however, strongly suppressed, leaving the proton-initiated radiation component as the dominating high energy emission mechanism.

3. Efficiencies and energetics

3.1. Proton radiation efficiency

The efficiency of producing photons from a proton of energy $\gamma_p m_p c^2$ within hadronic emission models is determined by the total photon production rate divided by the total proton loss rate r_{tot} :

$$\tilde{\xi}(\gamma_p) = \frac{\sum_i r_{i,photon}}{r_{tot}}$$

where loss rates include proton synchrotron, photomeson production, Bethe-Heitler pair production and adiabatic losses, and $\sum_i r_{i,photon}$ considers all processes that produce photons. By averaging over the input proton spectrum $\propto \gamma_p^{-p}$ the total radiation efficiency of protons is derived:

$$\xi_p = \frac{\int \tilde{\xi}_p(\gamma_p) \gamma_p^{1-p} d\gamma_p}{\int \gamma_p^{1-p} d\gamma_p}$$

(e.g., [33]). The evaluation of this formula is not trivial in the case of large magnetic field strengths where parts of the neutrino producing channels are re-directed to photon producing channels via significant synchrotron losses of secondary charged particles produced in photomeson production (e.g., μ , π , K , etc.). Radiation efficiencies from photomeson production have been estimated in the past with simplifying assumptions (e.g., neglecting the synchrotron channel of secondary charged particles) giving, for example, values of 1-10% in typical GRB environments (e.g., [18]) and even lower values for photomeson production in external only radiation fields of blazars (e.g., [40]). The fractional rate of photon production during one dynamical time scale after instantaneous injection of a power-law proton spectrum $\propto E^{-2}$ into a power-law radiation field of given density can also be derived directly from a given blazar model taking into account all radiation processes self-consistently. Depending on the chosen parameter set of the model we find [38] the radiation efficiency of protons in hadronic emission models to range from percent (e.g., for parameter settings with an early cutoff of the proton spectrum, or very low magnetic field values) to several tens of percent (e.g., for the case of a strong contribution from proton synchrotron radiation). The observed bolometric blazar luminosity can therefore be estimated by $L_{rad} \sim \Gamma_{10} \xi_p \xi_{conv,10} L_{jet}$ with Γ the bulk Lorentz factor $\Gamma = 10\Gamma_{10}$, ξ_p the proton radiation efficiency $\xi_p = 0.1\xi_{p,10}$, ξ_{conv} the efficiency of converting jet power into relativistic particle energies $\xi_{conv} = 0.1\xi_{conv,10}$, and L_{jet} the jet power. For a sufficient large jet power and favorable parameter choices typically observed blazar luminosities can therefore be accommodated in hadronic emission models.

3.2. Neutrino Production Efficiency and Fluxes

An inevitable by-product of hadronic interactions is the production of neutrinos. The prime neutrino production channel is here the decay of charged pions (π^\pm) and muons (μ^\pm). The

neutrino production efficiency in hadronic emission models is calculated by analogy with the photon production efficiency. Because of proton losses such as, e.g. proton synchrotron radiation, competing with photomeson production and π^\pm/μ^\pm -decay competing with synchrotron losses prior to its decay in highly magnetized environments it is clear that applying scaling relations to predict neutrino fluxes from gamma-ray observations can lead to neutrino flux upper limits only (e.g., Doert et al, this proceedings). We find [38] that in general the neutrino production efficiency is dependent on the model parameter values, reaching typically not more than $\sim 20\%$. It can be extremely low in the case of high field strengths and weak target photon fields (because of dominating proton synchrotron losses), and/or for low cutoff energies of the injected proton spectrum (threshold effect). Notably, in virtually no case is the neutrino production efficiency higher than the corresponding radiation efficiency.

Because of the potentially denser target photon field provided by powerful FSRQs as compared to BL Lacs, members of the former source class are considered a more promising neutrino source class as the close-by HSP-BL Lacs. Indeed, neutrino fluxes from typical HSP-BL Lacs can be several orders of magnitude lower than from FSRQs (e.g., 3C 279: [36]).

The predicted diffuse neutrino fluxes are also not only highly model-dependent but also suffer from large uncertainties (which can extend up to several orders of magnitude [30]) which originate from unknowns in the model parameters, uncertainties of the class luminosity functions and evolution, etc.

Current instruments are meanwhile capable of limiting the neutrino fluxes to not significantly above the ‘‘Waxman-Bahcall limit’’ (e.g., [1]) thereby ruling out hadronic neutrino production models with optimistically high predicted ν -fluxes.

4. Hadronic blazar modeling along the sequence HSP - ISP - LSP

There is overall consensus that synchrotron radiation from primary electrons dominates most parts of the low energy blazar SED in either model, leptonic or hadronic⁶. In the hadronic Synchrotron-Proton Blazar (SPB) model, e.g., the high energy bump stems mainly from direct proton, μ^\pm/π^\pm synchrotron radiation and their reprocessed components, and possibly contributions from the π -cascades [30]. Which of those processes dominate the SED at gamma-ray energies depends on the chosen parameter set. E.g., in environments with high field strengths but relatively weak low energy photon fields a dominance of proton synchrotron radiation is expected with a negligible cascading component. Such environments offer, e.g., the low-luminosity HSP-BL Lacs (e.g., PKS 2155-304: Fig. 6; [6]). By increasing the target photon density the probability of photomeson production and reprocessing increases. The resulting high energy SED appears smoother, often accompanied with a higher level of X-ray/soft gamma-ray emission. Because of the higher photomeson production losses the injected proton spectrum is expected to cut off earlier, as does the corresponding gamma-ray spectrum, in comparison to the case of very low photon densities. Examples may be the ISP-BL 3C 66A where the high energy radiation is found to be dominated by a heavily reprocessed proton synchrotron component [35], and the LSP-BL BL Lacertae where pion production losses are found to dominate over proton synchrotron losses with a resulting dominance of strongly reprocessed μ/π -synchrotron radiation at X- to gamma-rays (see Fig. 7; [14]). In the case of FSRQs additional external target photon fields may play a role in forming the overall gamma-ray spectrum also in hadronic emission models, although satisfactorily data representations by hadronic emission models with only internal target photon fields may be found as well (e.g., [15] where modellings of the 2006 flare of 3C 279 have been presented; see Fig. 8). The large observed luminosity of FSRQs require

⁶ Synchrotron radiation from secondary electrons may in some cases also contribute to the low energy hump in the SED .

then large jet powers in the framework of hadronic emission models (see Sect. 3). Because of the cascading of power from high to lower energies, a characteristic feature of hadronic emission models, gamma-ray spectra can naturally be extended to very high energies even with unusually hard spectral shapes (in the galaxy frame) also for FSRQs.

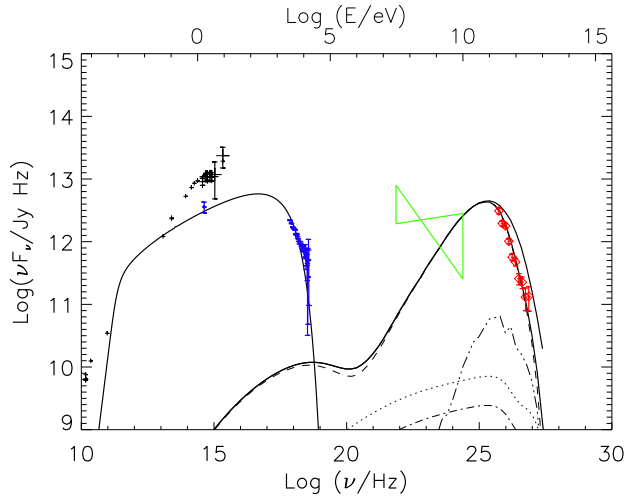


Figure 6. Hadronic SPB modeling of the quiescent state broadband SED in 2003 of the HBL PKS 2155-304 (see also [6]). Left solid line: synchrotron spectrum of primary electrons; right solid lines: emerging cascade spectrum and cascade spectrum corrected for absorption in the EBL. The dominant contribution to the high energy component is proton synchrotron radiation plus its reprocessed part (dashed line) while the contribution from μ synchrotron cascade (triple-dot-dashed line), π^0 cascade (dotted line), and π^\pm cascade (dot-dashed line) is negligible.

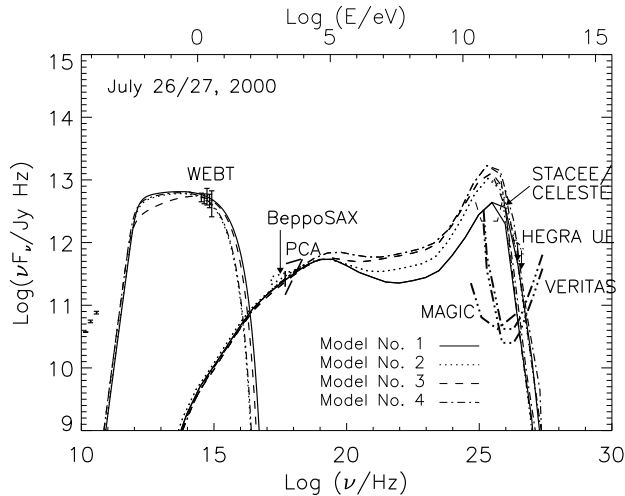


Figure 7. Various hadronic SPB model applications (corrected for absorption in the EBL) in comparison to the broadband SED data of July 2000 of the LBL BL Lacertae [14]. The μ synchrotron cascade contributes significantly to the high energy radiation component.

Acknowledgments

AR acknowledges support by Marie Curie IRG grant 248037 within the FP7 Program.

References

- [1] Abbasi R *et al*, (The IceCube collaboration) 2011 *Preprint* arXiv:1104.5187
- [2] Abdo A A *et al* (The Fermi-LAT collaboration) 2010a *ApJ* **722** 520

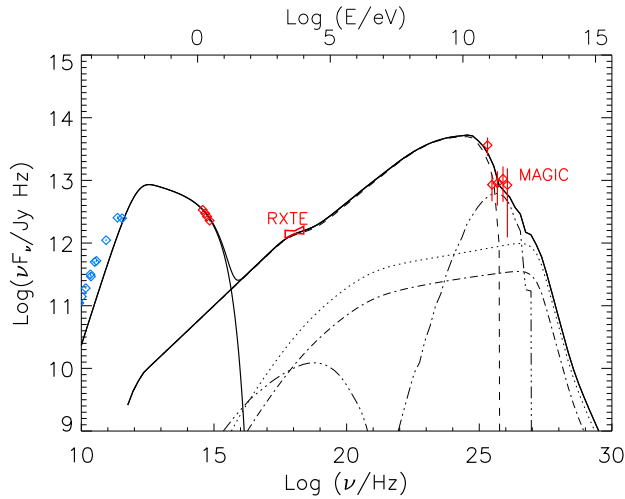


Figure 8. Hadronic SPB modeling of the broadband SED of 2006 of the FSRQ 3C 279 [15]. Left solid line: synchrotron spectrum of primary electrons; right solid line: emerging cascade spectrum (corrected for absorption in the EBL) as the sum of the proton synchrotron cascade (dashed line), μ synchrotron cascade (triple-dot-dashed line), π^0 cascade (dotted line), and π^\pm cascade (dot-dashed line). No external photon fields were used here. The proton and μ synchrotron cascades dominate the high energy radiation. See [15] for a SPB model fit where external BLR photons serve as an additional seed photon field.

- [3] Abdo A A *et al* 2010b (The Fermi-LAT collaboration) *ApJ* **715** 429
- [4] Abdo A A *et al* 2011 (The Fermi-LAT collaboration) *ApJ* in preparation
- [5] Aharonian F A 2000 *New Astr.* **5** 377
- [6] Aharonian F A *et al* (HESS collaboration), 2005, *A&A* **430** 865
- [7] Aharonian F A *et al* (HESS-collaboration) 2007 *ApJ Lett* **664** L71
- [8] Aharonian F A and Taylor A M 2010 *Aph* **34** 258
- [9] Albert J *et al* (MAGIC-collaboration) 2007 *ApJ* **669** 862
- [10] Atoyan A M and Dermer C D 2003 *ApJ* **586** 79
- [11] Barkov M V, Aharonian F A and Bosch-Ramon V 2010 *ApJ* **724** 1517
- [12] Bednarek W and Protheroe R J 1997 *MNRAS* **287** 9
- [13] Bednarek W & Protheroe R J 1999 *MNRAS* **302** 373
- [14] Böttcher M & Reimer A 2004 *ApJ* **609** 576
- [15] Böttcher M, Reimer A, & Marscher A 2009 *ApJ* **703** 1168
- [16] Celotti A and Ghisellini G 2008 *MNRAS* **385** 283
- [17] Dermer C D, Razzaque S, Finke J D, Atoyan A 2009 *New Journal of Physics* **11** 065016
- [18] Dermer C D 2010, Proc. of "The Shocking Universe: Gamma Ray Bursts and High Energy Shock Phenomena" Venice, Italy, September 2009
- [19] Eichler D & Wiita P J 1978 *Nature* **274** 38
- [20] Guo A and Mathews W G 2011 *ApJ* **728** 121
- [21] Hillas A M 1984 *Ann.Rev. A&A* **22** 425
- [22] Levinson A 2000 *PhRvL* **85** 912
- [23] Mannheim K and Biermann, P L 1992 *A&A* **253** 21
- [24] Medvedev M V 2000 *ApJ* **540** 704
- [25] Mücke A, Rachen J P, Engel R, *et al.* 1999 *PASA* **16** 160
- [26] Mücke A, Rachen J P, Engel R, *et al.* 2000 *NuPhS* **80** 08/10
- [27] Mücke A & Protheroe R J 2000 *AIPC* **515** 149
- [28] Mücke A, Engel R, Rachen J P, *et al.* 2000 *CoPhC* **124** 290
- [29] Mücke A and Protheroe R J 2001 *Aph* **15** 121
- [30] Mücke A, Protheroe R J, Engel R 2003 *et al.*, *Aph* **18** 593
- [31] Pohl M and Schlickeiser R 2000 *A&A* **354** 395 & Erratum: **355** 829
- [32] Protheroe R J 1997 *IAU Coll. 163* Vol. **121** 585
- [33] Protheroe R J & Mücke A 2001 ASP Conference Proceedings, 250, 113
- [34] Rachen J P and Meszaros P 1998 *Phys Rev D* **58** 123005
- [35] Reimer A, Joshi M, Böttcher M 2008 *AIP* **1085** 502
- [36] Reimer A 2009 *Int. Journal of Modern Physics D* **18** 1511
- [37] Reimer A and Böttcher 2012, in: "Relativistic Jets from Active Galactic Nuclei" ed M Böttcher, D Harris,

H Krawczynski (John Wiley & Sons) chapter 3

[38] Reimer A *et al* 2011, in preparation

[39] Sikora M and Madejski G M 2000 *ApJ* **534** 109

[40] Sikora M, Stawarz L, Moderski R, Nalewajko K and Madejski G 2009 *ApJ* **704** 38

[41] Urry C M and Padovani P 1995 *PASP* **107** 803

[42] Wilson A S, Smith David A, Young A J 2006 *ApJ* **644** 9